RSC Advances

PAPER

Ni^{3+} doped cobalt–nickel layered double hydroxides as high-performance electrode materials for supercapacitors†

H. M. Sun,[ab] Y. X. Ye,[a] Z. F. Tian,[a] S. L. Wu,[a] J. Liu [ID] *[a] and C. H. Liang[a]

Co–Ni layered double hydroxides (LDHs), as promising supercapacitor electrode materials with high specific capacity, have suffered from poor rate properties and cycling stability. Doping and topochemical oxidation of Ni ions is considered as an efficient route to overcome these drawbacks. In this work, Ni^{3+} doped cobalt–nickel layered double hydroxides (Co–Ni-LDHs) were synthesized by pulse laser ablation of a Ni target in CoCl$_2$ aqueous solution. The existence of Ni^{3+} ions doped in Co–Ni-LDHs decreases the conductive resistance, and increases the mobility of surface charge and transfer rate of the electrolyte. As a result, the Ni^{3+} doped Co–Ni-LDHs display a maximum specific capacitance of 2275 F g^{-1} and 1450 F g^{-1} at the current density of 1 A g^{-1} and 20 A g^{-1}, respectively, indicating a high rate of specific capacitance. Moreover, the capacitance retention is 80% after 1800 cycles at the current density of 6 A g^{-1}, manifesting good cycling stability of Ni^{3+} doped Co–Ni-LDHs.

Introduction

Transition metal-based layered double hydroxide materials (LDHs) are considered as one of the most promising materials for pseudocapacitors, owing to the low cost, environmental friendliness and high theoretical capacitance.[1–4] Compared to monometallic hydroxide, LDHs present two kinds of metal inserted in the host layer, which could provide richer redox reactions and offer an effective way of achieving improved electrochemical performance.[5,6] However, the poor rate capacitance and cycle stability due to the severe large volume expansion and the poor conductivity limit the practical applications of LDH structures for supercapacitor materials. To overcome these disadvantages, substantial efforts are focused on the efficient incorporation of highly conductive materials such as graphene, CNT, conductive polymers into the LDHs composites to improve the conductivity.[7,8] For example, Huang et al.[9] fabricated CoNiAl-LDH nanosheets attached on sandwich-like reduced graphene oxide (RGO) with 1866 F g^{-1} at the current density of 1 A g^{-1} while maintaining 1360 F g^{-1} at the current density of 10 A g^{-1}. Another strategy is to design hierarchical or porous structure with high surface area grown on the current collector (nickel foam,[10] conductive textile substrate[11]) to buffer the volume expansion.[12,13] But the low material loading masses are not suitable for the application.

Recently, engineering M^{3+} in LDHs phase has emerged as an effective approach to solving this problem. The M^{3+} (M = Ni, Co) species of LDHs play a key role in the efficiency of the active metal sites as well as controlling electron-transfer rate.[14–17] Wang[18] etched Al in Ni–Co–Al LDH by NaOH to enable the partial conversion of Co^{2+} to Co^{3+} with enhanced conductivity. Compared to Ni–Co–Al LDH, Ni–Co–Al LDHs after NaOH treatment display the lower resistance which lead to faster electrode kinetics. Moreover, theoretical studies[19] has demonstrated the spin-up states of Ni^{3+} in monolayer NiTi-LDH (0.9 nm) can improve density of states values around the Fermi level, demonstrating a half-metallic characteristic to improve carrier mobility and electrical conductivity. Therefore, M^{3+} in LDHs are desirable to improve electrochemical performance.[20,21] Although good results were obtained by doping M^{3+}, special chemical treatments to the precursor are generally needed to induce the transformation from M^{2+} to M^{3+}. For example, Co^{3+} doped layered double hydroxides were synthesized through a topochemical oxidative reaction employing bromine (Br$_2$),[22] O$_2$,[17] NO$_3^-$ ions[9] as an oxidizing agent, or chemical etching of Al in Ni–Co–Al LDH by NaOH.[10,20] Therefore, it still needs to explore a simple and green strategy method to synthesize M^{3+} doped layered double hydroxides materials.

Laser ablation in liquids (LAL) technique has been demonstrated a novel strategy to fabricate nanomaterials with the desired size, structures and components.[23–25] Also, it's an effective route to achieving doping ions into hydroxides. For

[a]Key Laboratory of Materials Physics, Anhui Key Laboratory of Nanomaterials and Nanotechnology, Institute of Solid State Physics, Chinese Academy of Sciences, Hefei 230031, China. E-mail: jliu@issp.ac.cn

[b]Department of Materials Science and Engineering, University of Science and Technology of China, Hefei 230026, China

† Electronic supplementary information (ESI) available: Fig. S1 laser-assisted assembly for Co–Ni-LDHs structure, Fig. S2 EDX spectrum and the table of corresponding elements calculation of Co$_{0.55}$Ni$_{0.45}$-LDHs, Fig. S3 XPS spectra of Co$_{0.55}$Ni$_{0.45}$-LDHs (a) survey, (b) O 1s 2p, Fig. S4 the specific capacitance retention of Co$_{0.55}$Ni$_{0.45}$-LDHs. See DOI: 10.1039/c7ra09427b

example, our group has fabricated Mn-doped $Ni(OH)_2$ nano-sheets,[26] Co-doped $Ni(OH)_2$ (ref. 27) by laser ablation of a Mn or Co target in $NiCl_2$ aqueous solution. In this work, by laser ablation of a Ni target in $CoCl_2$ aqueous solution, doping and topochemical oxidation of Ni^{3+} ions were simultaneously accomplished in one step. We successfully fabricated the Ni^{3+} doped cobalt–nickel layered double hydroxides (Co–Ni-LDHs). Moreover, as-synthesized Ni^{3+} doped Co–Ni-LDHs used as electrode materials for supercapacitors display high rate specific capacitance and excellent cycling stability.

Experimental

LAL assisted formation of Co–Ni-LDHs

As shown in Fig. S1,† firstly, a nickel target (99.99% in purity) is fixed in a vessel filled with 18 mL 0.01 M $CoCl_2$ solution, and ablated for 30 min by a Nd:YAG laser with wavelength of 1064 nm, pulse duration of 10 ns and per pulse laser energy of 120 mJ. The obtained colloidal solution was aged for 15 h. The precipitate is the final products, subsequently washed with ethanol and deionized water alternately for three times for characterization and application in supercapacitors.

Structural characterization of Co–Ni-LDHs

Scanning electron microscopy (SEM) system (Sirion 200 FEG) was used to observe the morphology of the Co–Ni-LDHs nano-structures. Energy dispersive X-ray spectrometry (EDX) was used to determine the element content. A transmission electron microscopy (TEM) system (JEOL, JEM-2010) with a 200 kV acceleration voltage was used to obtain the structural infor-mation of the products and element distribution. X-ray diffraction (XRD) analysis of the collected powder products was performed by using a Philips X'Pert system with Cu-Kα radiated ($\lambda = 1.5419$ Å). The surface chemical states were ana-lysed by X-ray photoelectron spectroscopy (XPS; Thermo ESCACLB 250). The surface area and porosity of the samples were measured using an Omnisorp 100CX Analyzer (Beckman Coulter, Inc., USA).

Supercapacitors performance of Co–Ni-LDHs

The as-prepared samples were used as electro-active materials for supercapacitors. The electrochemical performances of electrodes were evaluated on a Zahner electrochemical work-station (Germany) at room temperature and measured in 3 M KOH electrolyte. The working electrode was prepared by dispersing the samples into N-methyl pyrrolidone and mixed with polyvinylidene fluoride and acetylene black in a mass ratio of 8 : 1 : 1 and then painted on Ni foam. The mass loading of the powders on the nickel foam (1 cm × 1 cm) was determined by subtracting the weight before deposition from that after deposition and calculated to be around 3 mg cm^{-2}. The test system is a standard three-electrode configuration, including an Ag/AgCl electrode as a reference electrode and a platinum foil as the counter electrode. The specific capacitance of the electrode could be calculated according to eqn (1). Where C is the specific capacitance (F g^{-1}), I is the current density (A), t is the discharge

time (s), ΔV is the potential window (V), and m is the mass of the active materials (g), respectively.

$$C = \frac{It}{m\Delta V} \qquad (1)$$

Results and discussion

Fig. 1a presents the XRD pattern of as-synthesized Co–Ni-LDHs. The two prominent low-angle diffraction peaks located at 11.21° and 22.69° are assigned to (003) and (006) lattice planes of the hydrotalcite-like LDHs phase, which are similar to the standard XRD peaks for α-$Co(OH)_2$ phase (JCPDS no. 42-1467).[28] In addition, the (00h) reflections present sharp, symmetric and high diffraction intensity, suggesting that the synthesized structure is well crystallized with a regular interlayer and the preferential orientation growth along ⟨00h⟩ zone axis. Corre-sponding SEM and TEM image of Co–Ni-LDHs (Fig. 1c and d) show typical morphology of aggregated nanosheets that inter-connect with each other to form a porous structure. Calculated by the Barrett–Joyner–Halenda (BJH) model (Fig. 1b), the specific surface area and pore diameter is of 201.9 m^2 g^{-1} and 11.3 nm, respectively, which is much larger than that of $Ni(OH)_2$ nanosheets (114 m^2 g^{-1})[29] and floss-like Ni–Co binary hydrox-ides (106.5 m^2 g^{-1}).[30] Such large specific surface area and nanosheets-based porous structures allow high access of elec-trolyte to the integrated nanosheets, which is crucial for the reduction of the interface contact resistance between the elec-trodes and electrolyte.[31] TEM image of several separated nano-sheets (Fig. 1e) reveals a hexagonal shape of Co–Ni-LDHs, and the corresponding SAED pattern (inset in Fig. 1e) presents perfect hexagonal diffraction spots well matched with d-spacing of (110) lattice plane, indexed as the two-dimensional in-plane reflections. EDS spectrum (Fig. S2 in ESI†) of products demonstrates that the element ratio of Co and Ni is to be 0.55 : 0.45, thus it can be marked as $Co_{0.55}Ni_{0.45}$-LDHs. Also, the EDS elemental mapping images (Fig. 1f and g) verify that all elements (Co, Ni, and O) are uniformly distributed in $Co_{0.55}Ni_{0.45}$-LDHs.
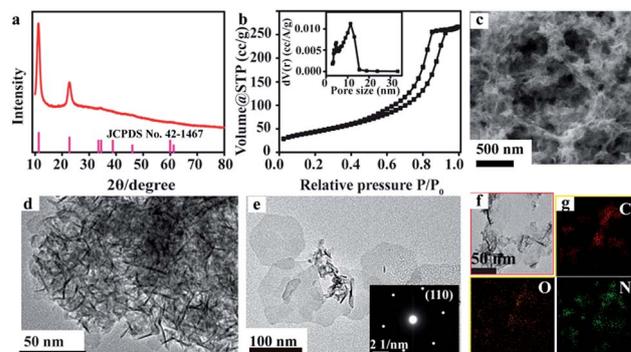

Fig. 1 (a) XRD pattern of Co–Ni-LDHs, (b) N_2 adsorption desorption isotherms and pore-size-distribution curves of Co–Ni-LDHs, (c) SEM image of Co–Ni-LDHs, (d) TEM image of Co–Ni-LDHs, (e) TEM image and the corresponding SAED pattern of individual Co–Ni-LDHs nanosheets, (f and g) EDX elemental mapping images of Co–Ni-LDHs.
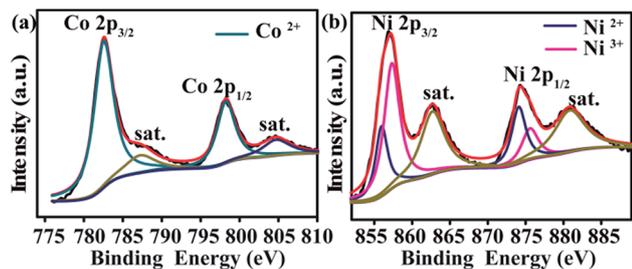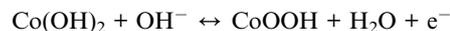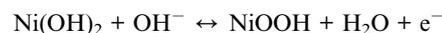
Fig. 2 XPS spectra of $Co_{0.55}Ni_{0.45}$-LDHs (a) Co 2p, (b) Ni 2p.

XPS spectra are used to analyse the valence states of $Co_{0.55}Ni_{0.45}$-LDHs. The C 1s peak at 284.8 eV is calibrated the binding energies of other elements. The survey XPS spectra of $Co_{0.55}Ni_{0.45}$-LDHs (Fig. S3a†) present sharp photoelectron peaks of Co, Ni, O and C elements. Fig. S3b† shows the fine XPS spectrum of O 1s, the peak located at 531.1 eV is related to hydroxyl ions.[35] In the Co 2p region (Fig. 2a), one pair of binding energies located at 782.5 eV and 798.5 eV coincide with Co^{2+}.[32,33] While in the Ni 2p region (Fig. 2b), two typical Ni^{3+} $2p_{3/2}$ and Ni^{2+} $2p_{3/2}$ peaks located at 856.3 eV and 855.9 eV are co-existed in the $Co_{0.55}Ni_{0.45}$-LDHs.[33] It means that Ni^{3+} ions are doped in $Co_{0.55}Ni_{0.45}$-LDHs, which is ascribed to the unique LAL reaction process described as follows. As pulse laser irradiating on the interface between Ni target and liquid, a plasma plume including atoms, ions, radicals and Ni^{3+}, Ni^{2+} with high temperature and high pressure is produced. Subsequent ultrasonic and adiabatic expansion of the hot plasma lead to a quick cooling of the plume region to form Ni clusters. The as-formed Ni clusters interacted with the surrounding aqueous solution, this processes involved in the generation of hydroxyl ions and the formation of the nuclei of Ni^{3+} doped $Co_{0.55}Ni_{0.45}$-LDHs which finally grow into network nanosheets.[34,35]

$Co_{0.55}Ni_{0.45}$-LDHs are used as electrode materials for supercapacitors, electrochemical performance are investigated by cyclic voltammetry (CV), galvanostatic charge–discharge

measurements. CV curves of $Co_{0.55}Ni_{0.45}$-LDHs (Fig. 3a) at the first test cycle present obvious redox peaks, revealing pseudo-capacitive characteristics, which differ from the nearly rectangular CV shapes for conventional EDLCs.[36] The reactions involved could be interpreted as follows:[37]

$$Ni(OH)_2 + OH^- \leftrightarrow NiOOH + H_2O + e^-$$

$$Co(OH)_2 + OH^- \leftrightarrow CoOOH + H_2O + e^-$$

$$CoOOH + OH^- \leftrightarrow CoO_2 + H_2O + e^-$$

In addition, CV curves within the potential window of 0.0–0.5 V (vs. Ag/AgCl) at various scan rates from 5 to 50 mV s^{-1} is evaluated and shown in Fig. 3b. With the rising of scan rate, the currents increase and the potentials of redox peaks shift to a more negative or positive position. This phenomenon is mainly due to the fact that the increasing of scan rate would cause the rising in the internal diffusion resistance within the pseudoactive materials.[38,39] Here, the good linear relationship between the oxidation peak currents and the square root of scan rates (Fig. 3c) confirms that the electrode reaction of $Co_{0.55}Ni_{0.45}$-LDHs is diffusion controlled.[40] Furthermore, even at the high scan rate of 50 mV s^{-1}, the shape of CV curve does not significantly distort, implying the nature of fast electron transport.

To further evaluate the rate capacity and cycling stability of the prepared $Co_{0.55}Ni_{0.45}$-LDHs, galvanostatic charge–discharge (GCD) measurements were conducted. Fig. 3d shows the GCD of the $Co_{0.55}Ni_{0.45}$-LDHs at different current densities from 1 A g^{-1} to 20 A g^{-1} in a voltage range of 0.1–0.5 V. The well-defined charge and discharge plateaus in all curves demonstrate the existence of redox reaction, confirming the previous CV results. The specific capacitance of the $Co_{0.55}Ni_{0.45}$-LDHs (Fig. 3e) composite is calculated to be 2275, 2153, 1965, 1845, 1708 and 1450 F g^{-1} at the current discharge of 1, 2, 4, 6, 10, and 20 A g^{-1} according to eqn (1). The specific capacitance retention of $Co_{0.55}Ni_{0.45}$-LDHs at different current densities is displayed in

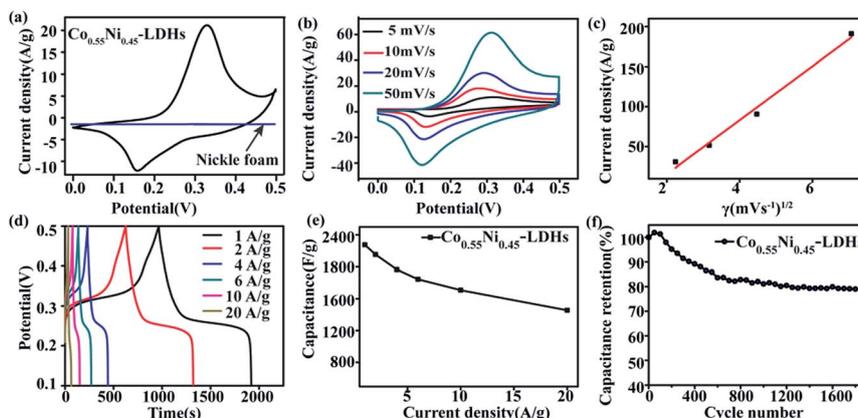Fig. 3 (a) CV curves of $Co_{0.55}Ni_{0.45}$-LDHs at scan rate of 5 mV s^{-1}, (b) CV curve of $Co_{0.55}Ni_{0.45}$-LDHs at various scan rates, (c) the linear relationship of $Co_{0.55}Ni_{0.45}$-LDHs between the oxidation peak currents and the square root of scan rates, (d) galvanostatic charge–discharge curves of $Co_{0.55}Ni_{0.45}$-LDHs at 1, 2, 4, 6, 10, and 20 A g^{-1}, (e) the specific capacitance of the $Co_{0.55}Ni_{0.45}$-LDHs at 1, 2, 4, 6, 10, and 20 A g^{-1}, (f) cycling performance at a scan rate of 6 A g^{-1} of $Co_{0.55}Ni_{0.45}$-LDHs.

Table 1 Comparison of various relative results of Co–Ni-LDHs

Material	Mass loading (mg)	Voltage range (V)	Specific capacitance (F g^{-1})	Current density (A g^{-1})	Ref.
Co$_{0.55}$Ni$_{0.45}$-LDHs	3	0.1–0.5	1708	10	This work
	3	0.1–0.5	1450	20	This work
Ni^{3+} doped NiTi-LDHs	2	0–0.45	1500	20	19
RGO@CoNiAl-LDHs	2	0–0.45	1360	10	8
α phase Ni–Co hydroxides	2–3	0–0.55	1350	20	33
Floss-like Ni–Co hydroxides	3	0–0.5	594	10	27
Ni(OH)$_2$ hexagonal platelets	3	0.6–0	628	10	39
CoNiAl-LDHs/GO	5	0.35 to −0.1	618	20	8

Fig. S4.† The high capacity retention of 64% is achieved for Co$_{0.55}$Ni$_{0.45}$-LDHs when the current density is increased from 1 A g^{-1} to 20 A g^{-1}, displaying high rate capability. Fig. 3f displays the cyclic performance of the obtained Co$_{0.55}$Ni$_{0.45}$-LDHs composite at a current density of 6 A g^{-1}. It can be seen that the specific capacitance shows a gradual decrease at first, and it is nearly constant after 800 cycles. After 1800 cycles, there is still 80% capacitance retention for Co$_{0.55}$Ni$_{0.45}$-LDHs electrode, indicating a good cycling stability.

In comparison with the previously reported results (Table 1), including RGO@CoNiAl-LDH,[9] floss-like Ni–Co binary hydroxides[30] and α phase Ni–Co bimetallic hydroxides,[36] here synthesized Co$_{0.55}$Ni$_{0.45}$-LDHs exhibit better specific capacitance. The achieved high specific capacitance, excellent rate capability and the long cycle life may be understood as following issues: (a) the Ni^{3+} promote electron transportation to reduce the conductivity of Co$_{0.55}$Ni$_{0.45}$-LDHs,[19] (b) the high specific surface area and porous structure of Co$_{0.55}$Ni$_{0.45}$-LDHs could shorten the diffusion distance between the electrolyte and electrodes, which can promote deep ions diffusion in electrochemical reaction,[32,41] (c) the uniform distribution of Ni is a key factor to ensure the electron transfer, which can effectively optimize the electrical conductivity and durability of the electrode materials.[21]

Conclusions

In summary, Ni^{3+} doped Co$_{0.55}$Ni$_{0.45}$-LDHs were prepared by liquid-phase laser ablation method. Detailed characterization reveals Ni^{3+} doped Co$_{0.55}$Ni$_{0.45}$-LDHs hexagonal sheet-like shape, high specific surface area, porous structures and uniform distribution of Co, Ni elements. As electrode materials for supercapacitors, Co$_{0.55}$Ni$_{0.45}$-LDHs yields a maximum specific capacitance of 2275 F g^{-1} at 1 A g^{-1}, and 1450 F g^{-1} at the high current density of 20 A g^{-1}, which indicates high rate capacity. Furthermore, Co$_{0.55}$Ni$_{0.45}$-LDHs present 80% capacitance retention after 1800 cycles at 6 A g^{-1}, meaning long cycle life for energy storage applications. Overall, this work provided a novel and efficient strategy in engineering M^{3+} in LDHs phase and confirmed that is an effective approach for improving their supercapacitor performance for practical energy storage devices.

Conflicts of interest

There are no conflicts to declare.

References

1 Y. Zhao, J. Liu, Y. Hu, H. Cheng, C. Hu, C. Jiang, L. Jiang, A. Cao and L. Qu, *Adv. Mater.*, 2013, **25**, 591.
2 J. Pu, Y. Tong, S. B. Wang, E. H. Sheng and Z. H. Wang, *J. Power Sources*, 2014, **250**, 250.
3 Z. Chen, Y. Qin, D. Weng, Q. Xiao, Y. Peng, X. Wang, H. Li, F. Wei and Y. Lu, *Adv. Funct. Mater.*, 2009, **19**, 3420.
4 R. Birjega, A. Matei, M. Filipescu, F. Stokker-Cheregi, C. Luculescu, D. Colceag, R. Zavoianu, O. D. Pavel and M. Dinescu, *Appl. Surf. Sci.*, 2013, **278**, 122.
5 R. R. Salunkhe, B. P. Bastakoti, C. T. Hsu, N. Suzuki, J. H. Kim, S. X. Dou, C. C. Hu and Y. Yamauchi, *Chem.– Eur. J.*, 2014, **20**, 3084.
6 W. L. Ma, L. Wang, J. Y. Xue and H. T. Cui, *J. Alloys Compd.*, 2016, **662**, 315.
7 L. Wang, D. Wang, X. Y. Dong, Z. J. Zhang, X. F. Pei, X. J. Chen, B. Chen and J. Jin, *Chem. Commun.*, 2011, **47**, 3556.
8 J. H. Fang, M. Li, Q. Q. Li, W. F. Zhang, Q. L. Shou, F. Liu, X. B. Zhang and J. P. Cheng, *Electrochim. Acta*, 2012, **85**, 248.
9 P. P. Huang, C. Y. Cao, Y. B. Sun, S. L. Yang, F. Wei and W. G. Song, *J. Mater. Chem. A*, 2015, **3**, 10858.
10 N. Abushrenta, X. C. Wu, J. N. Wang, J. F. Liu and X. M. Sun, *Sci. Rep.*, 2015, **5**, 13082.
11 G. N. Nagaraju, G. S. R. Raju, Y. H. Ko and J. S. Yu, *Nanoscale*, 2016, **8**, 812.
12 Q. B. Zhang, H. X. Chen, J. X. Wang, D. G. Xu, X. H. Li, Y. Yang and K. Zhang, *ChemSusChem*, 2014, **7**, 2325.
13 J. P. Cheng, J. H. Fang, M. Li, W. F. Zhang, F. Liu and X. B. Zhang, *Electrochim. Acta*, 2013, **114**, 68.
14 F. Gu, X. Cheng, S. F. Wang, X. Wang and P. S. Lee, *Small*, 2015, **11**, 2044.
15 P. Vialat, P. Rabu, C. Mousty and F. Leroux, *J. Power Sources*, 2015, **293**, 1.

16 V. M. Iluc, A. J. M. Miller, J. S. Anderson, M. J. Monreal, M. P. Mehn and G. L. Hillhouse, *J. Am. Chem. Soc.*, 2011, **13**, 13055.

17 P. Vialat, C. Mousty, C. Taviot-Gueho, G. Renaudin, H. Martinez, J. C. Dupin, E. Elkaim and F. Leroux, *Adv. Funct. Mater.*, 2014, **24**, 4831.

18 X. Wang, C. Y. Yan, A. Sumboja, J. Yan and P. S. Lee, *Adv. Energy Mater.*, 2014, **4**, 1301240.

19 Y. F. Zhao, Q. Wang, T. Bian, H. J. Yu, H. Fan, C. Zhou, L. Z. Wu, C. H. Tung, D. O'Hare and T. Zhang, *Nanoscale*, 2015, **7**, 7168.

20 X. L. Wu, L. L. Jiang, C. L. Long, T. Wei and Z. J. Fan, *Adv. Funct. Mater.*, 2015, **25**, 1648.

21 H. Chen, L. F. Hu, M. Chen, Y. Yan and L. M. Wu, *Adv. Funct. Mater.*, 2014, **24**, 934.

22 J. B. Liang, R. Z. Ma, N. B. Iyi, Y. S. Ebina, K. Takada and T. Sasaki, *Chem. Mater.*, 2010, **22**, 371.

23 H. M. Zhang, J. Liu, Y. X. Ye, Z. F. Tian and C. H. Liang, *Phys. Chem. Chem. Phys.*, 2013, **15**, 5684.

24 J. Liu, C. H. Liang, H. M. Zhang, Z. F. Tian and S. Y. Zhang, *J. Phys. Chem. C*, 2012, **116**, 4986.

25 J. Liu, C. H. Liang, G. P. Xu, Z. F. Tian, G. S. Shao and L. D. Zhang, *Nano Energy*, 2013, **2**, 328.

26 Z. F. Tian, C. H. Liang, J. Liu, H. M. Zhang and L. D. Zhang, *J. Mater. Chem.*, 2011, **21**, 18242.

27 D. W. Liang, S. L. Wu, J. Liu, Z. F. Tian and C. H. Liang, *J. Mater. Chem. A*, 2016, **4**, 10609.

28 Z. P. Liu, R. Z. Ma, M. Osada, K. Takada and T. Sasaki, *J. Am. Chem. Soc.*, 2005, **127**, 13869.

29 W. P. Sun, X. H. Rui, M. Ulaganathan, S. Madhavi and Q. Y. Yan, *J. Power Sources*, 2015, **295**, 323.

30 Y. F. Tang, Y. Y. Liu, W. C. Guo, S. X. Yu and F. M. Gao, *Ionics*, 2015, **21**, 1655.

31 J. C. Chen, C. T. Hsu and C. C. Hu, *J. Power Sources*, 2014, **253**, 205.

32 W. Quan, Z. L. Tang, Y. Hong, S. T. Wang and Z. T. Zhang, *Electrochim. Acta*, 2015, **182**, 445.

33 X. Q. Cai, X. P. Shen, L. B. Ma, Z. Y. Ji, C. Xu and A. H. Yuan, *Chem. Eng. J.*, 2015, **268**, 251.

34 X. Y. Liu, Y. Q. Gao and G. W. Yang, *Nanoscale*, 2016, **8**, 4227.

35 P. S. Liu, W. P. Cai and H. B. Zeng, *J. Phys. Chem. C*, 2008, **112**, 3261.

36 S. P. Simon and Y. Gogotsi, *Nat. Mater.*, 2008, **7**, 845.

37 D. D. Xia, H. C. Chen, J. J. Jiang, L. Zhang, Y. D. Zhao, D. Q. Guo and J. W. Yu, *Electrochim. Acta*, 2015, **156**, 108.

38 J. Li, M. Yang, J. Wei and Z. Zhou, *Nanoscale*, 2012, **4**, 4498.

39 L. J. Li, J. Xu, J. L. Lei, J. Zhang, F. McLarnon, Z. D. Wei, N. B. Li and F. S. Pan, *J. Mater. Chem A*, 2015, **3**, 1953.

40 Y. W. Li, J. H. Yao, C. J. Liu, W. M. Zhao, W. X. Deng and S. K. Zhong, *Int. J. Hydrogen Energy*, 2010, **35**, 2539.

41 S. D. Min, C. J. Zhao, Z. M. Zhang, G. R. Chen, X. Z. Qian and Z. P. Guo, *J. Mater. Chem.*, 2015, **3**, 3641.